2012

Carrier dynamics in bulk GaN

Patrick Ščajev
Vilnius University

Kęstutis Jarašiūnas
Vilnius University

Serdal Okur
Virginia Commonwealth University, okurs@vcu.edu

Ümit Özgür
Virginia Commonwealth University, uozgur@vcu.edu

Hadis Morkoç
Virginia Commonwealth University, hmorkoc@vcu.edu

Scajev, P., Jarasiunas, K., & Okur, S., et al. Carrier dynamics in bulk GaN. Journal of Applied Physics, 111, 023702 (2012).

Carrier dynamics in bulk GaN

Patrik Ščajev,[1,a)] Kęstutis Jarašiūnas,[1,2] Serdal Okur,[2] Ümit Özgür,[2] and Hadis Morkoç[2]
[1]*Institute of Applied Research, Vilnius University, Saulėtekio Ave. 9-III, Vilnius 10222, Lithuania*
[2]*Department of Electrical and Computer Engineering, Virginia Commonwealth University, Richmond, Virginia 23284, USA*

(Received 12 September 2011; accepted 3 December 2011; published online 19 January 2012)

Carrier dynamics in hydride vapor phase epitaxy grown bulk GaN with very low density of dislocations, $5–8 \times 10^5$ cm^{-2}, have been investigated by time-resolved photoluminescence (PL), free carrier absorption, and light-induced transient grating techniques in the carrier density range of 10^{15} to $\sim 10^{19}$ cm^{-3} under single and two photon excitation. For two-photon carrier injection to the bulk (527 nm excitation), diffusivity dependence on the excess carrier density revealed a transfer from minority to ambipolar carrier transport with the ambipolar diffusion coefficient D_a saturating at 1.6 cm^2/s at room temperature. An extremely long lifetime value of 40 ns, corresponding to an ambipolar diffusion length of 2.5 μm, was measured at 300 K. A nearly linear increase of carrier lifetime with temperature in the 80–800 K range and gradual decrease of D pointed out a prevailing mechanism of diffusion-governed nonradiative recombination due to carrier diffusive flow to plausibly the grain boundaries. Under single photon excitation (266 and 351 nm), subnanosecond transients of PL decay and their numerical modeling revealed fast processes of vertical carrier diffusion, surface recombination, and reabsorption of emission, which mask access to pure radiative decay. © *2012 American Institute of Physics*. [doi:10.1063/1.3673851]

I. INTRODUCTION

Carrier dynamics in GaN are usually investigated by above-bandgap femtosecond or picosecond laser pulses. The high absorption coefficient, endemic to direct bandgap semiconductors in general and GaN in particular, results in high photogenerated carrier densities within the top 50 to 100 nm thick surface region (at 267 or 355 nm excitations, respectively) with carrier densities up to 10^{19} cm^{-3}. Consequently, nonlinear recombination and diffusion as well as bandgap renormalization (BGR) effects may take place, mainly during the initial stages of carrier decay. Vertical diffusion of the carriers from the surface towards the depth of the sample rapidly dilutes the injected ambipolar plasma density by an order of magnitude in a few hundred picoseconds and diminishes the impact of nonlinear processes.[1] Moreover, the diffusive flow in thick and low-defect density hydride vapor phase epitaxy (HVPE) crystals [with diffusion length of a few μm at room temperature (RT)] extends the carriers far away from the surface. As a result, their vanishing contribution to the band-edge luminescence leads to non-exponential photoluminescence (PL) transients.[2,3]

Two-photon (2P) excitation at below-bandgap (E_g), with excitation photon energy $E_g > h\nu > E_g/2$, is inherently more advantageous over the above-bandgap excitation,[4] but has not been fully utilized in the past. Low and moderate excess carrier densities (10^{15} to $\sim 10^{18}$ cm^{-3}) achievable in 2P excitation[2,5] allow one to avoid the nonlinear effects endemic to high-density plasma and eliminate inhomogeneous carrier spatial profiles. Therefore, the nonradiative recombination and carrier transport can be investigated with better accuracy in a wide range of temperatures and injection levels, which allows one to investigate the contributions of the extended and point defects.

There have been only a few reports comparing the carrier dynamics at one- and two-photon excitations in free-standing GaN. The initial PL decay time at room temperature was reported to be a few times slower for the 2P case (1100 ps) as compared to one-photon (1P) excitation (440 ps) (Ref. 2) and attributed to nonradiative carrier capture. In contrast, much longer PL decay times under 2P excitation of bulk GaN (from 2 ns at low temperatures to $\sim$17 ns at RT) were noted as exciton radiative time, while the nonradiative recombination time was not reported and the free-exciton and exciton-longitudinal optical (LO) phonon emission decay rates were assumed equal.[5] While the true radiative time of free exciton varied from 1.4 ns up to 9 ns at RT in 1 mm-thick GaN (Ref. 6), the initial $\sim$100 ps no-phonon PL component was tentatively attributed to surface states. An earlier study of radiative lifetime pointed out a correlation of exciton radiative lifetime with layer thickness and an estimated 3.5 ns lifetime in a 1 μm thick epilayer.[7]

Clearly, the reported rather scattered lifetime values and variety of recombination processes involved require further studies of carrier dynamics by complementary optical techniques, in order to delineate the role of nonradiative and radiative decays as well as diffusion processes. In this work, a bulk GaN crystal with low dislocation density ($5–8 \times 10^5$ cm^{-2}) was chosen in order to create more favorable conditions for radiative processes to become dominant, and facilitate the investigation of spatial and temporal carrier dynamics for different excitation conditions (e.g., single and two-photon carrier injection) in a wide temperature range (80 to 800 K). The analysis is complemented by numerical calculations of carrier dynamics under the excitation conditions employed.

[a)]Author to whom correspondence should be addressed. Electronic mail: patrik.scajev@ff.vu.lt.

II. EXPERIMENTAL TECHNIQUES

The sample used in this study is a $d = 200$ μm thick HVPE-grown GaN (electron concentration and mobility are $n_0 = 1.3 \times 10^{16}$ cm^{-3}, $\mu_n = 1200$ cm^2/Vs, respectively[8]). The single- and two-photon excitation utilized either 12 ps pulses at $\lambda_{3h} = 351$ nm, 15 ps pulses at $\lambda_{2h} = 527$ nm, or 150 fs pulses at 267 nm. Time-resolved free-carrier absorption (FCA) (Ref. 9), light-induced transient grating (LITG) (Refs. 10 and 11), and photoluminescence[3] techniques were applied for investigation of spatial and temporal carrier dynamics. The LITG technique paves the way for the determination of carrier diffusion coefficient and mobility, while the FCA decay provides the carrier recombination times. The FCA and LITG measurements were performed in the 80–800 K range. The standard setup of time-resolved PL spectroscopy was employed at room temperature using ~150 fs frequency-tripled pulses from a Ti-Sapphire laser along with a Hamamatsu streak camera.

The single-photon (1P) injection conditions allow one to study nonequilibrium carrier dynamics in the $\Delta N \sim 10^{17}$–5×10^{19} cm^{-3} carrier density range. In order to reduce the injected carrier density to the 10^{15}–3×10^{17} cm^{-3} range, two photon carrier generation was used. In 2P excitation, the 2nd harmonic pulse ($\tau_{2h} = 15$ ps at full width at 1/e intensity) of a Nd:YLF laser (operating at $\lambda_1 = 1053$ nm with 10 Hz repetition rate) generated the carriers in the bulk, and the recombination and diffusion processes were monitored by a delayed probe beam at longer wavelengths (1053 or 1064 nm). The optically delayed (up to 4 ns) picosecond probe pulse at $\lambda_1 = 1053$ nm was used to measure the fast decay transients. For the measurement of longer relaxation tails (hundreds of ns), an electronically delayed ~2 ns duration probe pulse at 1064 nm was generated from a diode-pumped Nd:YAG laser, triggered by the Nd:YLF laser.[9] The thickness of the photoexcited region δ under 2P excitation was three orders of magnitude larger ($\delta = \alpha^{-1}{}_{2P} \approx 100$ μm at 1 GW/cm^2 power density) when compared to the 1P injection case ($\delta = \alpha^{-1}{}_{1P} \approx 100$ nm at 351 nm with a diffusion-expanded photoexcited region of a few micrometers[1]). Therefore, to ensure detection of $\Delta N \times \delta$, which is the measured quantity, at low excess carrier density (i.e., at ΔN below 10^{17}–10^{18} cm^{-3}), two-photon excitation was required to increase the photoexcited thickness δ.

A. Light-induced transient grating technique

For grating recording, the excitation beam at wavelength $\lambda_{2h,3h}$ passed a diffractive optical element (a permanent diffraction grating with a fixed spatial period), and the two first order diffracted beams, intersecting at an angle Θ, provided an interference pattern with a period $\Lambda \approx \lambda_{2h,3h}/\sin(\Theta)$ on the sample.[11] The pump beam penetration depth under 1P excitation, $\alpha^{-1}{}_{1P}$, was determined by the interband absorption coefficient, and the carrier density near the surface was calculated as $N_{01P} = \alpha_{1P} I_0/h\nu$,[12] where α is the interband absorption coefficient, $I_0 = (1-R)I_{inc}$ is the excitation energy density in the sample (in mJ/cm^2), R is the reflection coefficient, I_{inc} is the incident excitation density, and $h\nu$ is the photon energy. Under two photon excitation, a value of two-photon coefficient β [cm/GW] and the excitation beam instantaneous power density[12] $P(t) = 2I_0 \exp(-4t^2/\tau^2{}_{2h})\pi^{-1/2}\tau_{2h}{}^{-1}$ [GW/cm^2] determine the generated carrier density $N_{02P} = \int_{-\infty}^{+\infty} \beta P(t)^2 dt/2h\nu = bI_0^2/2h\nu$. The factor $b = \beta/(\tau_{2h}\sqrt{\pi/2})$ describes a decrease of the incident fluence $I(z)$ during propagation inside the crystal,

$$I(x,z) = \frac{I(x)}{1 + bzI(x)}, \tag{1}$$

where $I(x) = I_0[1 + \cos(2\pi x/\Lambda)]$ (x is the direction of the grating vector $K = 2\pi/\Lambda$) and leads to a slightly decreasing carrier density $\Delta N(z)$ with the depth z,

$$\Delta N(x,z) = \frac{N_{02P}[1 + \cos(2\pi x/\Lambda)]^2}{(1 + bzI(x))^2}. \tag{2}$$

The above relationships allowed us to calculate an average carrier density $N_{av} = 1.5N_{02P}/[1 + bdI_0]$ for which the diffusion coefficient was measured (see Eq. (7)). The carrier density equals to N_{01P} and $1.5N_{02P}$ near the excited surface (at 1P and 2P injection condition, respectively), and the factor 1.5 is due to the nonsinusoidal profile of the grating at 2P excitation (see Eq. (2)).

The generated carriers lead to a refractive index change, $\Delta n = n_{eh}\Delta N$, according to Drude-Lorentz model,[10] where $n_{eh} = -e^2\lambda_1^2/(8\pi^2c^2n_1\varepsilon_0 m^*_{eh}) \times E_g^2/(E_g^2 - (hc/\lambda_1)^2)$ is the refractive index change per one electron-hole pair, $n_1 = 2.3$ is the refractive index for probe wavelength λ_1, ε_0 is the vacuum permittivity, $E_g = 3.4$ eV is the GaN bandgap, and m^*_{eh} is the reduced electron-hole effective mass [$1/m^*_{eh} = (1/m^*_e + 1/m^*_h)$]. A value of $n_{eh} = -1.36 \times 10^{-21}$ cm^{-3} was calculated for GaN using averaged $m_e = 0.2$ m_0 (Ref. 13) and $m_h = 1.5$ m_0 (Ref. 14).

The refractive index spatial modulation $\Delta n(x)$ creates a phase grating in the GaN crystal, on which the probe beam diffracts with efficiency $\eta(t)$,

$$\eta(t) = \left(\frac{2\pi n_{eh} N_{02P} d}{\lambda_1}\right)^2 \exp\left(-\frac{2t}{\tau_G}\right), \tag{3}$$

and provides the grating decay time τ_G,

$$\frac{1}{\tau_G} = \frac{1}{\tau_R} + \frac{1}{\tau_D}, \tag{4}$$

where τ_R and $\tau_D = \Lambda^2/4\pi^2 D$ are the carrier lifetime and diffusive decay time for the given diffusion coefficient D and grating period Λ. Equation (3) slightly overestimates the diffraction efficiency η due to depletion of pump beam (i.e., $I(z)$ and $\Delta N(z) \propto I(z)^2$ vary with depth at two-photon absorption conditions); therefore, numerical calculations provided the η decrease (with respect to Eq. (3)) of more than 50% at excitations above 15 mJ/cm^2. The exact value of the first order diffraction efficiency at arbitrary modulation profile $\Delta n(x,z,t)$ was calculated numerically according to Ref. 10,

$$\eta(t) = \left|\frac{2\pi}{\lambda_1}\int_0^{\Lambda}\int_0^{d} \Delta n(x,z,t)\, dz\, \cos\left(\frac{2\pi x}{\Lambda}\right) dx\right|^2. \tag{5}$$

This equation was used for fitting the measured dependence $\eta(I_0)$. For determination of D, the grating decay rates $1/\tau_G$ were measured at two different grating periods ($\Lambda = 1.74$ and 7.8 μm) in order to separate the diffusive and the recombinative contributions. The diffusive decay is always dominant at $\Lambda = 1.74$ μm period [according to Eq. (4)], as the measured carrier lifetime in bulk GaN was much longer, i.e., $\tau_R \gg \tau_D$; $\tau_R \approx 10$–100 ns in the 10–800 K range, and the corresponding $\tau_D \approx 0.3$–1 ns (see Secs. III B and III C). Moreover, the measured η value at a fixed excitation fluence ($\eta \propto \Delta N^2$) allowed determination of the two-photon absorption coefficient [see Eqs. (3) and (5)].

B. Free-carrier absorption technique

The FCA decay kinetics at 2P injection were used to determine carrier lifetime values τ_R at various temperatures and excitation densities. The carriers were injected by a single Gaussian beam, and the induced absorption transient, $\Delta\alpha(t) = \sigma_{eh}\Delta N(t)$, was monitored via the measurements of IR probe beam differential transmission $[T_0 - T(t)]/T_0 \propto 1 - \exp[-\Delta\alpha(t)d]$ (Ref. 15). At two photon excitation, the following general equation describes the FCA decay:

$$\ln(T_0/T(t)) = \sigma_{eh} d \frac{N_{02P}\exp(-t/\tau_R)}{1 + bdI_0}. \quad (6)$$

The dependence of FCA signal on the injected carrier density (at $t = 2\tau_{3h} \approx 24$ ps, following the excitation pulse) allowed determination of the free carrier absorption cross section $\sigma_{eh} = \ln[T_0/T(t = 2\tau_{3h})]/(N_{02P}d)$. This relationship is valid for relatively low fluences ($I_0 < 10$ mJ/cm^2) when the factor $bdI_0 \ll 1$. At higher I_0, the depth-averaged carrier density for both FCA ($N^* = N_{02P}$) and LITG ($N^* = 1.5N_{02P}$) techniques was calculated using

$$N_{av} = \int_0^d \Delta N^2(x,z)dz \Big/ \int_0^d \Delta N(x,z)dz \approx N^*/(1 + bdI_0). \quad (7)$$

C. Time-resolved photoluminescence technique

For TRPL measurements, the decay transients were detected by a UV sensitive streak camera system for excess carrier densities in the range 10^{16} to $\sim 10^{18}$ cm^{-3} (estimated at the very surface of GaN at the wake of the excitation pulse). For 1P injection, the carrier density near the surface is calculated as $\Delta N = \alpha I_0/h\nu$, where α is the interband absorption coefficient 2×10^5 cm^{-1} (Ref. 16) at 266 nm wavelength. Complementary to TRPL, the FCA decay measurements were performed at 1P carrier injection using 351 nm wavelength (at which $\alpha = 1 \times 10^5$ cm^{-1}).

III. RESULTS AND DISCUSION

A. Carrier density scaling

The two-photon absorption in GaN was confirmed by a nearly quadratic increase of the differential transmission (DT $\propto {I_0}^2$) associated with the nonlinear carrier generation rate $\Delta N \propto {I_0}^2$ (see Fig. 1). The grating diffraction efficiency, η, increased twice steeper than DT with excitation fluence ($\eta \propto {I_0}^4$). A slight deviation of the experimental power indices (${I_0}^\gamma$) of these dependences from the predicted by Eq. (3) values ($\gamma_{exp} < \gamma$, see Fig. 1) is due to the depletion of the excitation beam. The relationships between DT and η signals and the carrier density (Eqs. (1) to (6)) allowed determination of the free carrier absorption cross-section $\sigma_{eh} = (2.5 \pm 0.5) \times 10^{-17}$ cm^2 at 1053 nm and the two-photon absorption (TPA) coefficient $\beta = 15 \pm 2$ cm/GW at 527 nm (the factor b in Eq. (1) is equal to 0.85 cm/mJ). A similar β value of 17–20 cm/GW at 527 nm was obtained by Z-scan technique.[17] The fitting of dependence $\eta(I_0)$ allowed us to obtain $bdI_0 = 0.34$ (at 20 mJ/cm^2), which led to the depth averaged carrier density of $0.77 \times 1.5N_{02P}$ and $0.77N_{02P}$ for diffraction (LITG) and free carrier absorption, respectively. Therefore, depletion of the pump beam with depth provided the slightly decreased slopes γ with injection, as seen in the dependences in Fig. 1, for $I_0 \geq 5$–10 mJ/cm^2. The TPA coefficient was found virtually independent of temperature (within 10% error) as followed from the dependence of diffraction efficiency on T. On the other hand, the FCA cross-section had weak temperature dependence with T^s ($s = -0.15$) both for 1P and 2P excitations. The small σ value points out to carrier scattering being predominantly by polar optical phonons[18] as predicted by the relationship $\sigma_{eh} \sim T^0 h\nu^{-2.5}$.[19]

B. Ambipolar and hole diffusivity at two photon excitation

Two photon band-to-band excitations create holes and electrons with equal densities; therefore, the Dember field between the photoexcited carriers ensures that the electrons and holes diffuse together with the diffusion coefficient given as[20]

$$D(\Delta N) = (n_0 + \Delta N_n + \Delta N_h)D_n D_h / [(n_0 + \Delta N_n)D_n + \Delta N_h D_h]. \quad (8)$$

Noting that the hole mobility is much smaller than that of electrons ($D_h \ll D_n$), the measurements at the moderate excitation

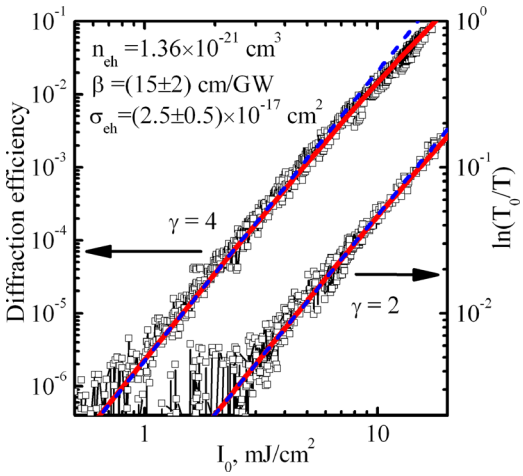

FIG. 1. (Color online) Dependences of light-induced diffraction efficiency, η, and differential transmission DT on excitation energy fluence, I_0, in GaN under two-photon carrier injection. The indices γ are the slopes of the curves in log-log scale: expected ones ($\gamma = 2$ and 4, dashed lines) and experimental ($\gamma_{exp} < \gamma$, solid lines). Notice the deviation from expected behavior with increasing excitation fluence.

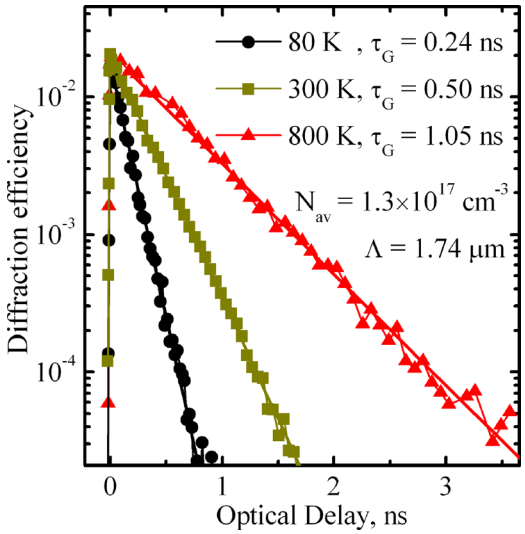

FIG. 2. (Color online) Diffusive decay of LITG kinetics for two-photon carrier injection in bulk GaN with a grating period of 1.74 μm. Various decay times reveal dependence of diffusivity on temperature.

regime ($\Delta N = \Delta N_n = \Delta N_h \gg n_0$) may provide an ambipolar diffusion coefficient D_a, while at low injection conditions ($\Delta N \ll n_0$), the hole diffusivity may be determined. Both cases were realized experimentally, assuming that $n_0 \sim 10^{16}$ cm^{-3} is a standard value for undoped HVPE GaN.[8] The small grating periods, Λ, ensured faster diffusive decay than the recombination governed decay ($\tau_D \ll \tau_R$), thus a plot of $1/\tau_G$ vs. $1/\Lambda^2$ for different Λ values (or even a single decay time $\tau_D = \Lambda^2/4\pi^2 D$) provided D at various injected carrier densities and temperatures. In Fig. 2, the exponential decay of the LITG at 2P carrier injection is plotted for a fixed grating period $\Lambda = 1.74$ μm at different sample temperatures. Similar measurements resulted in a set of diffusivity values for various injected carrier densities (Fig. 3(a)). The latter data at moderate excitation ($\Delta N_n = \Delta N_h = 10^{17}$ cm$^{-3} \gg n_0$) provided the $D_a \approx 2D_h = 1.6$ cm^2/s value as well as a hole mobility $\mu_h = D_a e/2kT = 31$ cm^2/Vs. On the other hand, deviation from ambipolarity at low excitations ($\Delta N_n = \Delta N_h = 10^{15}$ cm$^{-3} < n_0$) directly led to the hole mobility. We note that the excitation level at which $D_a = 1.5D_h$ corresponds to the doping concentration n_0 (see Eq. (8)), and thus the fitting of $D(\Delta N)$ curve allowed estimation of the equilibrium carrier density $n_0 \approx 8 \times 10^{15}$ cm^{-3} at RT.

For modeling of diffusivity dependence on injection at different temperatures (Fig. 3(a)), the equilibrium carrier densities are needed. These values were calculated using a previously determined donor concentration of 1.04×10^{16} cm^{-3} and acceptor of 2.4×10^{15} cm^{-3} (Ref. 21) (with activation energies $E_D = 25$ meV and $E_A = 140$ meV). The concentration of free electrons *vs.* T was calculated accordingly,[22] revealing its decrease to 3.2×10^{15} cm^{-3} at 80 K and saturation above RT at $n_0 = N_d - N_a = 8 \times 10^{15}$ cm^{-3}. In order to fit the hole diffusion coefficient temperature dependence (Fig. 3(b)), temperature-dependent scattering rates (see $D_{h,theor}$ in Eq. (9)) were used for acoustic (ac), polar and nonpolar optical phonon (pop and npo, respectively) scattering. Applicable equations[5] and the following appropriate parameters[9,21] were used for $D_{h,theor}$ calculation: static and optical dielectric constants $\varepsilon_r(0) = 10.4$, $\varepsilon_r(\infty) = 5.43$, density $\rho = 6.1$ g/cm^3,

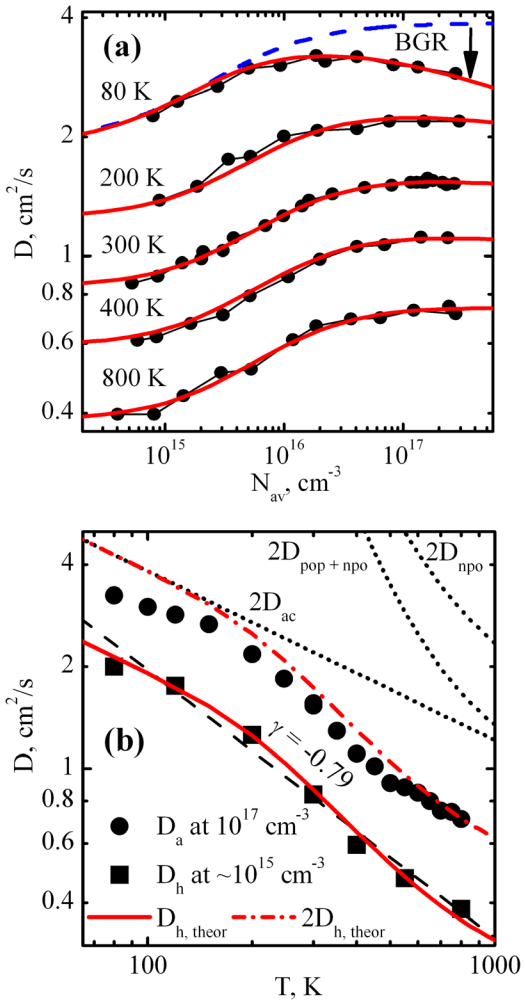

FIG. 3. (Color online) (a) The measured dependences of diffusivity D on injected carrier density at different temperatures (symbols) and the modeled data (solid curves); at 80 K, the modeled curves with/without the impact of band gap renormalization (BGR) are compared. (b) Experimental data compared with theoretically calculated temperature dependence for hole ($D_{h,\ theor}$) and ambipolar ($D_a = 2D_{h,\ theor}$) diffusivity (solid and dash dot curves, respectively), which account for acoustic (ac) and polar and nonpolar optical phonon (pop and npo, respectively) scattering (dotted curves). $\gamma = 0.79$ is the average slope (dashed line) of the dependence $D_h(T)$ in the log-log plot.

longitudinal sound velocity $v_{||} = 8$ km/s, heavy and light hole density of states effective masses $m_{HH/LH} = 1.9/0.33$ m_0 (Ref. 14), polar and nonpolar optical phonon energies 91 meV and 80 meV, respectively,[23] and fitted acoustic and optical inter/intra-valley deformation potentials, $C_a = 9.6$ eV and $D_{ii+jj} = 1.34 \times 10^9$ eV/cm, respectively. The dependence $D_{h,theor}$ was fitted by the empirical (with 2% precision) relationship $1/D_{h,theor} = 1/D_{ap} + 1/D_{op}$, where the $D_{ap} = 19.1 \times T^{-1/2}$ and $D_{op} = 3.6 \times 10^{-4} \times T[\exp(-E_{ph}/kT) - 1]$ correspond to acoustic and optical phonon ($E_{ph} = 91$ meV) contributions, respectively.

The carrier-density dependent ambipolar diffusion coefficient in GaN was calculated using the relationship $\Delta E_v(\Delta N) = Z \times [3\text{ meV } (\Delta N/10^{18})^{1/3} + 19\text{ meV } (\Delta N/10^{18})^{1/4}]$ (Ref. 24) for valence band modulation, which takes into account the effect of BGR by adjusting the fitting parameter Z. This factor $Z = 0.48$ for GaN is lower than that for SiC ($Z = 1$) probably due to higher density of valence band states as well as the larger static dielectric constant $\varepsilon_r(0) = 10.4$ in

GaN (as opposed to 9.66 in SiC) which reduce the BGR effect.[24–26]

The fundamental relations[25,27] allowed simulation of temperature and density dependent hole diffusivity in the nondegenerate regime (this approach is valid in the whole temperature range, because even at 80 K the density of states $N_{DOS} = 5.5 \times 10^{18}$ cm^{-3} value for holes is by an order of magnitude higher than the injected carrier density),

$$D_h = D_{h,theor}\left(1 + \frac{\Delta N}{kT}\frac{\partial \Delta E_v}{\partial \Delta N}\right), \quad \text{where}$$
$$D_{h,theor} = \frac{kT}{m_h}\int_0^\infty \left(\sum\nolimits_i \tau_i^{-1}(\xi,T)\right)^{-1} \xi^{3/2} e^{-\xi} d\xi \Big/ \int_0^\infty \xi^{3/2} e^{-\xi} d\xi. \tag{9}$$

Here, $\xi = E/kT$, E is the kinetic energy, and τ_i^{-1} is the appropriate hole scattering rate.[28]

At lower temperatures, the spatial bandgap renormalization[24] hindered carrier diffusion, and thus led to lower than calculated D_a values which manifested itself as decreasing $D(\Delta N)$ with increasing carrier density at 80 K (Fig. 3(a)). Moreover, the difference between $D_a = 2D_{h,\,theor}(T)$ dependence, not accounting for BGR, and the experimentally measured $D_a(T)$ at $T < 150$ K is also caused by BGR (Fig. 3(b)).

C. Carrier lifetime at two photon generation

Decay of FCA exhibited single exponential kinetics in the 80–800 K range and led to carrier lifetime τ_R which varied from ~10 to 120 ns with temperature (Fig. 4(a)). The lifetime was found to be independent of the excess carrier density in the range $\Delta N = 3 \times 10^{16}$–$5 \times 10^{17}$ cm^{-3} achieved at 2P injection conditions. The contribution of radiative recombination to the total carrier lifetime $1/\tau_R = 1/\tau_{Rad} + 1/\tau_{nRad}$, where τ_{Rad} and τ_{nRad} are the radiative and nonradiative lifetimes, respectively, was estimated to be minor, pointing to nonradiative origin of decay ($\tau_R = \tau_{nRad}$) (i.e., $1/\tau_{Rad} = B\Delta N \approx$ (2–5) $\times 10^{-11}$ cm^3 s$^{-1} \times 10^{17}$ cm^{-3} = (200–500 ns)$^{-1}$, using the radiative coefficient B values from Refs. 29 and 30.

The extremely long τ_R value at RT and unusual $\tau_R(T)$ dependence (Fig. 4(b)), incongruous with the expected Shockley-Read-Hall recombination rate, required a more detailed analysis of the recombination mechanism. Assuming that the dislocations are the most effective centers of nonradiative recombination and using an empirical relationship between the threading dislocation density N_{TD} and carrier lifetime, $\tau_R = kN_{TD}^{-1/2}$,[31] we estimated that $N_{TD} = 8 \times 10^5$ cm^{-2} corresponds to a lifetime of $\tau_R = 40$ ns. This dislocation density is close to that extracted by chemical etching and pit density analysis of similar samples (5×10^5 cm^{-2} on the Ga face[8]).

The observed almost inverse correlation between the $D_a(T)$ and $\tau_R(T)$ dependences (see Figs. 3(b) and 4(b)) exhibits features of surface recombination in a thin layer. Note that when the carriers are created inside the thick crystal of thickness d, their surface lifetime τ_S is dependent on the rate at which carriers diffuse from the photoexcited layer of thickness $2d^*$ to the surface ($\tau_{diff} \propto d^{*2}/D_a$) and recombine there with $\tau_{surf} \propto d^*/S$ (S is the surface recombination velocity).[9] In our case, the estimations for the studied 200 μm-thick layer provided $\tau_{diff} \approx 100$ μs which is far from reality ($D_a = 1.6$ cm^2/s value was used for the estimation). Therefore, diffusion to the internal boundaries of GaN hexagonal grains[32] (assumed to be cylinders of radius r_c for simplicity) must be considered, and τ_{surf} should be replaced with τ_{inter}, which depends on the interface recombination velocity S_{inter}. Using this model wherein $\tau_{Sinter} = \tau_{inter} + \tau_{diff} = \pi^{-1/2} r_c / S_{inter} + \pi^{-3/2} r_c^{\,2}/D_a$,[33] the fit of the measured τ_R value at RT (Fig. 4(b)) provided $r_c = 3.6$ μm and an effective interface recombination velocity of $S_{inter} = 9500$ cm/s at RT. Following this model, we fitted the experimentally measured temperature dependence of lifetime ($\tau_R \propto T^{1.15}$), inclusive of the defect related part, $\tau_{inter} \propto T^{3/2}$, which corresponds to a capture of carriers by charged defects with their cross section strongly dependent on temperature, $\sigma_c \sim T^{-2}$.[19] Consequently, the interface recombination rate rapidly decreases with temperature, $1/\tau_{inter} = \sigma_c v_{th} N_{tr} \sim T^{-3/2}$, where $v_{th} \sim T^{1/2}$ is the carrier thermal velocity and N_{tr} is the interface trap density. Therefore, the extended defects (dislocations) and associated point defects near the grain boundaries must be assumed as effective "interface" centers of nonradiative recombination for the carriers reaching them by diffusion. While this qualitative model accounts for the observed long

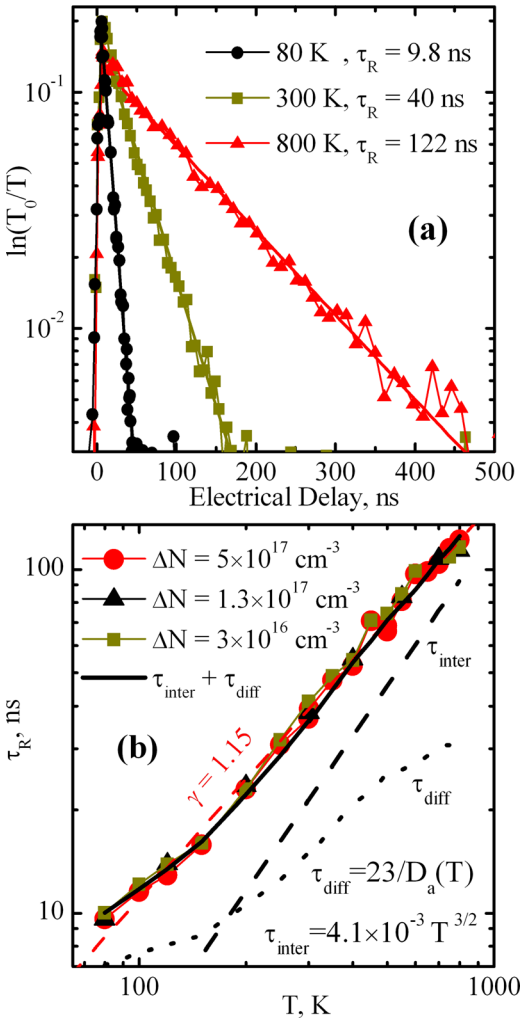

FIG. 4. (Color online) Kinetics of FCA decay at various temperatures (a) and carrier lifetime vs. temperature for different injection levels (b). Fitting of $\tau_R(T)$ is composed of diffusion and interface defect governed recombination terms.

carrier lifetimes, further spatially and time-resolved investigations of carrier dynamics in the vicinity of grain boundaries are warranted. We note that a similar correlation between the lifetime and diffusion temperature dependences was recently observed in bulk SiC crystals,[34] in which the nonradiative recombination at extended defects is known to be dominant.

D. PL transients at interband excitation

The room temperature TRPL kinetics were measured at $\sim 10^{18}$ cm^{-3} carrier injection by ~150 fs pulses of 267 nm wavelength. Complementary to TRPL, the LITG decay measurements were performed at 1P carrier injection using 12 ps pulses at 351 nm wavelength providing carrier densities up to 2×10^{19} cm^{-3}).

A deeper analysis of the PL and LITG kinetics was undertaken with the help of the numerical solution[1,9] to the continuity equation,

$$\frac{\partial N(z,t)}{\partial t} = D(\Delta N)\nabla^2 \Delta N(z,t) - \frac{\Delta N(z,t)}{\tau_R} - B\Delta N^2(z,t) + G(z,t), \quad (10)$$

where $G(z,t)$ is the carrier generation rate and B is the radiative recombination coefficient. The carrier density and its evolution was calculated assuming carrier injection by a 150 fs laser pulse at 267 nm and using the boundary condition D_a $\delta\Delta N(0,t)/\delta z = S\Delta N(0,t)$ at the front surface (z = 0) and the determined $D(\Delta N)$ and τ_R values. The instantaneous carrier spatial profiles $\Delta N(z)$ are shown in Fig. 5, providing impact of carrier diffusion and surface recombination. For calculation of the PL transients, the intensity of the PL emission was integrated over the excited layer thickness taking into account reabsorption of light emission α_R,[1]

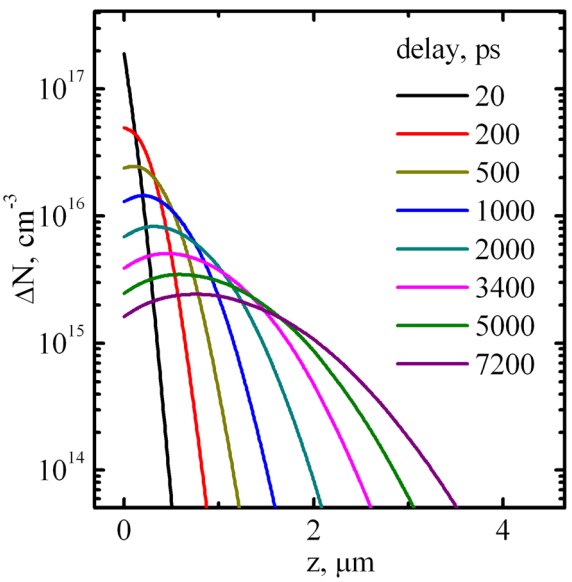

FIG. 5. (Color online) Evolution of carrier depth profiles in bulk GaN after carrier injection to a 50 nm thick layer by a Ti-sapphire laser pulse at 267 nm wavelength. Surface recombination velocity $S = 1.1 \times 10^4$ cm/s and D value varying from the ambipolar to the monopolar one (depending on the instant carrier density as determined before) were used for calculations.

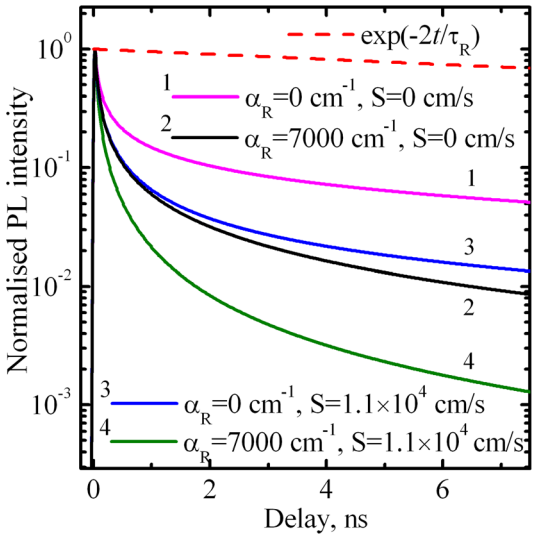

FIG. 6. (Color online) The calculated TRPL kinetics revealing impact of cases involving only diffusion ($\alpha_R = 0$, S = 0), diffusion and surface recombination ($\alpha_R = 0$, S ≠ 0), diffusion and reabsorption ($\alpha_R \neq 0$, S = 0), and all three factors, diffusion, surface recombination, and reabsorption ($\alpha_R \neq 0$, S ≠ 0). The expected slow PL decay component, governed by bulk recombination only ($I_{PL} \propto \exp(-2t/\tau_R)$ with $\tau_R = 40$ ns) is shown by a dashed line.

$$I_{PL} \propto \int_0^d \Delta N_p(\Delta N_n + n_0)\exp(-\alpha_R z)dz. \quad (11)$$

It was found that the initial fast PL decay within the first 100–500 ps has its genesis in the carrier diffusion away from the surface deeper into the sample which distributes the carriers over a ~1 μm depth within 1 ns. Ambipolar diffusion reduces the peak value of ΔN by an order of magnitude (from $\sim 10^{17}$ cm^{-3} at the end of laser pulse to $\sim 10^{16}$ cm^{-3} at $t = 1$ ns) (Fig. 5). At later times, when carriers diffuse to the deeper layer, an impact of PL emission reabsorption becomes more pronounced (Fig. 6), particularly for the shorter wavelengths (see PL decay rate in Fig. 7). Moreover, the surface recombination also contributes to PL decay, and fitting of the data revealed $S = 1.1 \times 10^4$ cm/s. Calculated transients using different α_R and S values are presented in Fig. 6. The data reveal the combined effects of PL reabsorption and/or surface recombination. One can then conclude that the fast diffusion-driven PL decay transient during of the initial 1 ns period cannot be avoided, while the subsequent decay transients (up to 10 ns) may be influenced both by PL reabsorption and surface states of GaN. We note that radiative recombination rate in the range of measured PL decay (~1.5 ns) was masked by faster processes of diffusion, surface recombination, and reabsorption, which decorated the initial PL decay and diminished the radiative component significantly.

The calculation of LITG decay kinetics (Fig. 7) also revealed the impact of surface recombination with the fitted $S = 3 \times 10^4$ cm^{-1}. The slightly higher S value (with respect to one for PL decay) may be due to an increase of S with injection.[6,9] We also assume that a rather large S value for the investigated bulk GaN might be influenced by the chemical mechanical polishing and subsequent long-term surface self-oxidation. On the other hand, contribution of bimolecular recombination at excess carrier density of 2×10^{19}

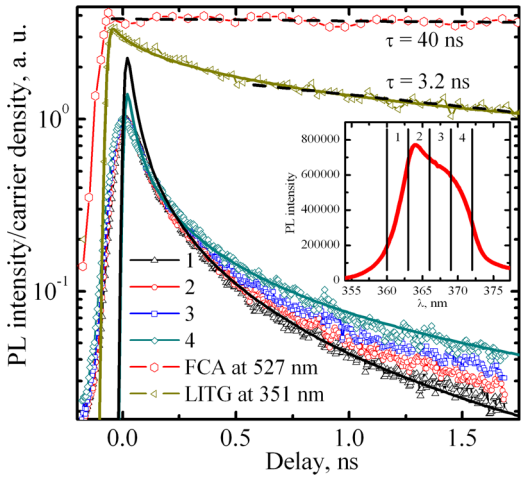

FIG. 7. (Color online) Comparison of carrier decay transients revealed by various optical techniques at single and two-phonon excitation conditions. PL transients recorded upon carrier injection to a thin surface layer by a strongly absorbed laser pulse (single photon carrier injection conditions). The inset shows the time-integrated PL spectrum, where the four spectral regions used to obtain the PL transients are marked. TRPL decays for four spectral regions (1 to 4) are compared with the calculated best fits (solid lines) using reabsorption coefficients of 7000 and 400 cm^{-1} in spectral regions 1 and 4, respectively, and $S = 1.1 \times 10^4$ cm/s. The recombination-governed LITG decay (grating period $\Lambda = 7.8$ μm), at 1P injection conditions, 2×10^{19} cm^{-3}, leads to carrier density decay instantaneous time of 3.2 ns (dashed line). For comparison, FCA decay at 2 P injection conditions (10^{17} cm^{-3}) indicates a 40 ns lifetime (dashed line).

cm^{-3} cannot be neglected in the LITG decay ($\tau_{Rad} = 1/B\Delta N \approx 5$ ns). As LITG decay with ps-pulse injection enables complete elimination of in-depth diffusion,[1] the observed grating decay rate at $t > 1$ ns (Fig. 7) seems to be influenced both by the surface and bimolecular recombination.

In short, the subnanosecond TRPL transients are consistent with the nonequilibrium carrier governed processes when the reabsorption and surface recombination are taken into consideration. The diffusion expands the spatial profile, and surface-related recombination rate has a strong impact as the very thin surface layer is photoexcited in the PL case. Moreover, the specificity of the PL technique (reabsorption of emission) also strongly modifies the PL kinetics. These peculiarities mask the excitonic emission features which should be observed in PL kinetics even at RT. We assume that the relatively high carrier density in the performed PL study slightly above $\sim 10^{18}$ cm^{-3} as well as the rather large surface recombination velocity for the investigated bulk GaN are the main factors/obstacles, which should be eliminated in further attempts of studying coexisting excitonic and free carrier mechanisms.

IV. CONCLUSIONS

Direct measurements of carrier dynamics in a high quality bulk GaN at two-photon excitation have shown that nonequilibrium processes in the entire 80–800 K range and moderate excitations (from 10^{15} to 10^{17} cm^{-3}) can be reliably analyzed by a model of free-carrier plasma. The study provided minority and ambipolar carrier mobilities (31 and 60 cm^2/V s), a nonradiative recombination rate of 2.5×10^7 s^{-1}, and an ambipolar carrier diffusion length of 2.5 μm at RT. Extremely long lifetime values, varying from 40 ns at 300 K to 120 ns at 800 K, were measured by the free carrier absorption technique. The lifetime increased nearly linearly with temperature, whereas the ambipolar carrier diffusivity showed an opposite trend, decreasing with temperature in the same temperature range. This anticorrelation pointed out that dominant nonradiative recombination pathway is most likely due the extended defects (dislocations) and associated point defects near the grain boundaries, acting as effective "interface" nonradiative centers for the carriers reaching them by diffusion. The corresponding interface recombination velocity was determined to be 9400 cm/s. The ambipolar diffusion coefficient was observed to saturate at $D_a = 1.6$ cm^2/s at room temperature under high injection (10^{17} cm^{-3}) and was as high as 3.2 cm^2/s at 80 K, decreasing slightly with increased injection beyond 2×10^{16} cm^{-3} due to band gap renormalization.

Nonequilibrium carrier dynamics at single photon excitation at 267 nm was explored through time-resolved photoluminescence and transient grating decay. The subnanosecond PL transients revealed carrier diffusion away from the photoexcited thin surface region and surface recombination, which diminished the emission signal essentially, preventing direct access to radiative relaxation. Transient grating decay was less sensitive to the surface recombination due to deeper carrier injection at 351 nm and not sensitive to carrier in-depth diffusion, therefore an impact of bimolecular recombination was observed.

ACKNOWLEDGMENTS

Research at Vilnius University was partially funded by TAP 5/2011 project of the Lithuanian Science Council. Virginia Commonwealth University acknowledges support from AFOSR and NSF Grants. K.J. acknowledges sponsorship of the Baltic-American Freedom Foundation (BAFF/CIEE).

[1]T. Malinauskas, K. Jarašiūnas, S. Miasojedovas, S. Juršėnas, B. Beaumont, and P. Gibart, Appl. Phys. Lett. **88**, 202109 (2006).
[2]S. Juršėnas, S. Miasojedovas, A. Žukauskas, B. Lucznik, I. Gregory, and T. Suski, Appl. Phys. Lett. **89**, 172119 (2006).
[3]Ü. Özgür, Y. Fu, Y. T. Moon, F. Yun, H. Morkoç, and H. O. Everitt, J. Appl. Phys. **97**, 103704 (2005).
[4]H. Yang, S. J. Xu, Q. Li, and J. Zhang, Appl. Phys. Lett. **88**, 161113 (2006).
[5]Y. Zhong, K. S. Wong, W. Zhang, and D. C. Look, Appl. Phys. Lett. **89**, 022108 (2006).
[6]B. Monemar, P. P. Paskov, J. P. Bergman, A. A. Toropov, T. V. Shubina, T. Malinauskas, and A. Usui, Phys. Status Solidi B **245**, 1723 (2008).
[7]J. S. Im, A. Moritz, F. Stauber, V. Härle, F. Scholtz, and A. Hangleiter, Appl. Phys. Lett. **70**, 631 (1997).
[8]M. A. Reshchikov, H. Morkoç, S. S. Park, and K. Y. Lee, Appl. Phys. Lett. **78**, 3041 (2001); *ibid.* **81**, 4970 (2002).
[9]P. Ščajev, V. Gudelis, K. Jarašiūnas, and P. B. Klein, J. Appl. Phys. **108**, 023705 (2010).
[10]H. J. Eichler, P. Günter, and D. W. Pohl, *Laser-Induced Dynamic Gratings* (Springer, Berlin, 1986).
[11]K. Jarašiūnas, R. Aleksiejūnas, T. Malinauskas, V. Gudelis, T. Tamulevičius, A. Guobienė, A. Usikov, V. Dmitriev, and H. J. Gerritsen, Rev. Sci. Instrum. **78**, 033901 (2007).
[12]C. Klingshirn, *Semiconductor Optics* (Springer, Berlin, 2005).
[13]V. Bougrov, M. E. Levinshtein, S. L. Rumyantsev, and A. Zubrilov, *Properties of Advanced Semiconductor Materials GaN, AlN, InN, BN, SiC, SiGe*, edited by M. E. Levinshtein, S. L. Rumyantsev, and M. S. Shur (Wiley, New York, 2001), pp. 1–30.
[14]Y. C. Yeo, T. C. Chong, and M. F. Li, J. Appl. Phys. **83**, 1429 (1998).

[15]J. Linnros, J. Appl. Phys. **84**, 275 (1998).
[16]J. F. Muth, J. H. Lee, I. K. Shmagin, and R. M. Kolbas, Appl. Phys. Lett. **71**, 2572 (1997).
[17]V. Pačebutas, A. Stalnionis, A. Krotkus, T. Suski, P. Perlin, and M. Leszczynski, Appl. Phys. Lett. **78**, 4118 (2001).
[18]E. Kioupakis, P. Rinke, A. Schleife, F. Bechstedt, and C. G. Van de Walle, Phys. Rev. B **81**, 241201(R) (2010).
[19]B. K. Ridley, *Quantum Processes in Semiconductors* (Clarendon, Oxford, 1999).
[20]J. F. Schetzina and J. P. McKelvey, Phys. Rev. B **2**, 1869 (1970).
[21]D. Huang, F. Yun, M. A. Reshchikov, D. Wang, H. Morkoç, D. L. Rode, L. A. Farina, Ç. Kurdak, K. T. Tsen, S. S. Park, and K. Y. Lee, Solid State Electron. **45**, 711 (2001).
[22]J. Pernot, W. Zawadzki, S. Contreras, J. L. Robert, E. Neyret, and L. Di Cioccio, J. Appl. Phys. **90**, 1869 (2001).
[23]H. Siegle, G. Kaczmarczyk, L. Filippidis, A. P. Litvinchuk, A. Hoffmann, and C. Thomsen, Phys. Rev. B **55**, 7000 (1997).
[24]C. Persson, U. Lindefelt, and B. E. Sernelius, Solid State Electron. **44**, 471 (2000).
[25]J. F. Young and H. M. Driel, Phys. Rev. B **26**, 2147 (1982).
[26]T. Malinauskas, K. Jarašiūnas, E. Ivakin, N. Tranchant, and M. Nesladek, Phys. Status Solidi A **207**, 2058 (2010).
[27]H. Iwata and K. M. Itoh, J. Appl. Phys. **89**, 6228 (2001).
[28]J. Pernot, S. Contreras, and J. Camassel, J. Appl. Phys. **98**, 023706 (2005).
[29]A. Dmitriev and A. Oruzheinikov, J. Appl. Phys. **86**, 3241 (1999).
[30]T. Malinauskas, K. Jarašiūnas, R. Aleksiejūnas, D. Gogova, B. Monemar, B. Beaumont, and P. Gibart, Phys. Status Solidi B **243**, 1426 (2006).
[31]K. Jarašiūnas, T. Malinauskas, S. Nargelas, V. Gudelis, J. V. Vaitkus, V. Soukhoveev, and A. Usikov, Phys. Status Solidi B **247**, 1703 (2010).
[32]N. G. Weimann and L. F. Eastman, J. Appl. Phys. **83**, 3656 (1998).
[33]P. Ščajev, A. Usikov, V. Soukhoveev, R. Aleksiejūnas, and K. Jarašiūnas, Appl. Phys. Lett. **98**, 202105 (2011).
[34]P. Ščajev, J. Hassan, K. Jarašiūnas, M. Kato, A. Henry, and P. Bergman, J. Electron. Mater. **40**, 394 (2011).